Journal of Microscopy, Vol. 224, Pt 2 November 2006, pp. 166–180
Received 11 March 2006; accepted 18 May 2006

Calibration of a wide-field frequency-domain fluorescence lifetime microscopy system using light emitting diodes as light sources

A. D. ELDER, J. H. FRANK*, J. SWARTLING, X. DAI & C. F. KAMINSKI
Department of Chemical Engineering, University of Cambridge, Pembroke Street, Cambridge, U.K.
**Sandia National Laboratories, Livermore, California, U.S.A.*

Summary

High brightness light emitting diodes are an inexpensive and versatile light source for wide-field frequency-domain fluorescence lifetime imaging microscopy. In this paper a full calibration of an LED based fluorescence lifetime imaging microscopy system is presented for the first time. A radio-frequency generator was used for simultaneous modulation of light emitting diode (LED) intensity and the gain of an intensified charge coupled device (CCD) camera. A homodyne detection scheme was employed to measure the demodulation and phase shift of the emitted fluorescence, from which phase and modulation lifetimes were determined at each image pixel. The system was characterized both in terms of its sensitivity to measure short lifetimes (500 ps to 4 ns), and its capability to distinguish image features with small lifetime differences. Calibration measurements were performed in quenched solutions containing Rhodamine 6G dye and the results compared to several independent measurements performed with other measurement methodologies, including time correlated single photon counting, time gated detection, and acousto optical modulator (AOM) based modulation of excitation sources. Results are presented from measurements and simulations. The effects of limited signal-to-noise ratios, baseline drifts and calibration errors are discussed in detail. The implications of limited modulation bandwidth of high brightness, large area LED devices (~40 MHz for devices used here) are presented. The results show that phase lifetime measurements are robust down to sub ns levels, whereas modulation lifetimes are prone to errors even at large signal-to-noise ratios. Strategies for optimizing measurement fidelity are discussed. Application of the fluorescence lifetime imaging microscopy system is illustrated with examples from studies of molecular mixing in microfluidic devices and targeted drug delivery research.

Correspondence to: C. F. Kaminski. Tel: +44 (0)1223 763135; fax: +44 (0)1223 334796; e-mail: cfk23@cam.ac.uk

Introduction

Fluorescence lifetime imaging microscopy (FLIM) is a powerful tool in the analytical sciences, opening up a parameter space not accessible for probing with techniques that solely measure fluorescence intensities (Suhling & Stephens, 2006). The fluorescence lifetime is a sensitive indicator of a fluorophore's interactions with molecules in the immediate environment. The emission lifetime can yield information on conformational changes in macromolecules (Calleja *et al.*, 2003), molecular association such as protein binding events (Vermeer *et al.*, 2004), changes in local pH (Lin *et al.*, 2003), diffusional mobility (Clayton *et al.*, 2002), the presence of quenchers such as oxygen or ions (Szmacinski *et al.*, 1995) and many other parameters (Lakowicz, 1999). In addition, fluorescence lifetime differences can be used to distinguish between fluorophores that are spectrally indistinguishable (Dowling *et al.*, 1998).

Lifetime imaging microscopy can be performed in either the time domain or the frequency domain. For time domain measurements, short pulses of excitation light are used, and the fluorescence emission is measured as a function of time. Conventionally, the time at which the intensity falls to 1/e of its initial value is defined to be the fluorescence lifetime. For widefield microscopy, gated detection with intensified CCD cameras has been used for lifetime measurements (Periasamy *et al.*, 1996; Dowling *et al.*, 1997). Good temporal resolution at the subnanosecond level requires very fast intensifiers (Dowling *et al.*, 1999). One disadvantage in most implementations of this technique is that the signal is sampled only for a fraction of the emission time, resulting in a loss of photons, although more photon-efficient schemes are possible in certain circumstances (Ballew & Demas, 1989).

For point scanning devices, time correlated single photon counting (TCSPC) is widely employed (Becker *et al.*, 1999, 2004). The sample is illuminated by a series of short light pulses, and the arrival time of individual photons following each pulse is recorded. The technique provides very high

precision and accuracy, permitting multiple exponential decays to be differentiated (Volkmer *et al.*, 2000) and has matured to such a level that operation close to theoretically achievable efficiencies is possible. The technique is ideally matched to technology for two-photon laser scanning microscopy (Denk *et al.*, 1990), which requires short pulse length, high repetition rate laser sources for excitation. The titanium : sapphire laser has become mainstream technology for two photon microscopy, due to its high peak power and wide tuning range, matching the spectra of a vast number of biological fluorophores (So *et al.*, 1994). New excitation sources, such as pulsed diode lasers (Kress *et al.*, 2001) and supercontinuum sources (Dunsby *et al.*, 2004), are now entering the market and can be used for one- and two-photon excited TCSPC. A disadvantage of TCSPC is that the photon signal count rate must be kept significantly below the excitation pulse rate (typically by a factor of 20–100) such that 'pile-up' is prevented and photon arrival times can be correctly assigned. The TCSPC signal is accumulated until a sufficient number of photons are collected for a precise determination of the local lifetime (Köllner & Wolfrum, 1992). The low signal rate combined with the sequential nature of signal acquisition for laser scanning microscopes can lead to unacceptable acquisition times for some dynamic applications such as *in vivo* imaging or microfluidic applications.

Frequency domain FLIM (FD-FLIM) measurements are performed by periodic intensity modulation of the excitation source and homodyne (or heterodyne) phase sensitive detection (Lakowicz, 1999; Lakowicz *et al.*, 1992). This technique is usually implemented in the wide-field imaging mode, although it has been used in point scanning devices, including two-photon microscopes (So *et al.*, 1995) and a recent application involving the use of telecommunications type ultrafast superheterodyne detection technology (Booth & Wilson, 2004). The latter has been shown capable of performing real time FD-FLIM at rates compatible with point scanning confocal systems. The original implementation of FD-FLIM by Lakowicz *et al.* (Lakowicz & Berndt, 1991) used picosecond laser pulse trains for fluorophore excitation and a radio-frequency (rf) modulated intensified CCD camera. Traditionally, FD-FLIM systems have, like TCSPC, required expensive laser excitation technology such as high repetition rate pulsed lasers or rapidly modulated cw lasers. The advent of inexpensive light emitting diodes (LEDs) is expected to boost interest in the technique by greatly reducing the cost of FLIM technology, especially if unintensified rapid modulation gain camera systems become available (Mitchell *et al.*, 2002). The wavelength range covered by diodes spans the entire visible spectrum, and LEDs with improved spectral brightness and stability are entering the market all the time at ever decreasing costs (Dasgupta *et al.*, 2003). The wavelength range is continuously being pushed further into the UV spectral region (McGuinness *et al.*, 2004) opening potential for intrinsic protein fluorescence excitation. Herman *et al.* (Herman *et al.*, 2001) describe the first implementation of such technology based on diode sources emitting near 370 and 460 nm. Their method used a point scanning approach and gain modulated PMTs for detection, limiting the resolution to around 15 μm. Recently, very high brightness diodes have become available permitting high power wide-field illumination over almost the entire visible range (www.luxeon.com).

In this paper, we assess a FD-FLIM system that employs a high brightness LED for excitation and a gain modulated image intensifier in front of a CCD camera (van der Oord *et al.*, 2001; van Geest & Stoo, 2003). An advantage of this system is the rapid acquisition speed, as lifetime information is simultaneously collected in parallel on all image pixels. However, the lifetime resolution is limited due to the relatively low modulation bandwidth achievable with large area LED devices. Here we report on the calibration of such a system and discuss issues of resolution and minimum resolvable lifetime differences. We calibrate the system using a similar procedure as described by Hanley *et al.*, (2001) and compare the results to independent measurements performed using other techniques including TCSPC, time gated detection, and acousto-optical modulator (AOM) based FD-FLIM systems. Issues of finite modulation bandwidths and measurement noise are addressed in terms of minimum resolvable lifetime differences, and strategies are suggested to optimize system performance. Finally, we show and discuss applications of the device for lifetime measurements in microfluidic devices and live cells.

Background

In FD-FLIM, an excitation source illuminates the sample with a time modulated intensity, and the fluorescence signal exhibits a phase shift and a demodulation relative to the illuminating radiation. For each harmonic component of the excitation light at angular frequency, ω, the phase shift, ϕ, and the relative demodulation, m, in the signal are related to the fluorescence lifetime, τ, by Eqs (1) and (2), respectively:

$$\phi = \tan^{-1}(\omega\tau) \tag{1}$$

$$m = (1 + \omega^2\tau^2)^{-1/2} \tag{2}$$

Phase shift and demodulation can be measured using a gain modulated detection device operating at a frequency at or near to, ω, and acquiring images at different phase delays between excitation and detection waveforms (homodyne or heterodyne detection, respectively) (Gadella *et al.*, 1993). To account for the phase shift and demodulation that are introduced by the electronics and optics, it is usually necessary to perform measurements relative to a reference sample with a known fluorescence lifetime, τ_{ref}, using the following equations:

$$\tau_\phi = \frac{1}{\omega}\tan\left((\phi - \phi_{ref}) + \tan^{-1}(\omega\tau_{ref})\right) \tag{3}$$

$$\tau_m = \frac{1}{\omega}\left(\frac{m_{\text{ref}}^2}{m^2}(1+\omega^2\tau_{\text{ref}}^2)-1\right)^{1/2} \quad (4)$$

where ϕ_{ref}, m_{ref} and τ_{ref} refer to the phase shift, demodulation and lifetime of the reference and τ_ϕ and τ_m are referred to as the phase and modulation lifetimes, respectively. Lifetimes can thus be calculated independently from either the phase shift or the demodulation using Eqs (3) or (4), but only in the case of single exponential fluorescence decays is $\tau_\phi = \tau_m$. If multiple lifetime components are present, then τ_ϕ and τ_m represent weighted averages over all the lifetime components in the sample. Through a repetition of measurements at several modulation frequencies dispersion curves can be measured, from which the individual lifetime components can be recovered. At the low frequency end, both τ_ϕ and τ_m are biased towards the longest lifetime component present in the sample, whereas the converse is true at the high frequency end of the spectrum. Note that under special circumstances single frequency measurements can be used to differentiate lifetime components within a sample where only two lifetimes are present (Hanley & Clayton, 2005).

In most FD-FLIM work reported in the literature, either pulsed lasers or modulated cw lasers have been used as light sources. These approaches can offer flexibility in the choice of optimal modulation frequencies over a large bandwidth with maximum frequencies of several 100 MHz. Modulation depths of more than 100% have been achieved at multiple harmonics simultaneously by use of several modulation devices in series and exploitation of the nonlinear gain behaviour of image intensifiers. Such an approach permits precise determination and differentiation of multiple lifetime components in mixtures in single measurement runs (Squire *et al.*, 2000). Here we use LEDs, which are inexpensive and have excellent illumination characteristics for wide-field microscopy. A disadvantage of the LEDs is their limited modulation bandwidth. Modulation of LEDs is achieved through direct modulation of the diode injection current. The highest modulation frequency is limited by the capacitance of the device, which is determined by charge capacitance associated with the p-n junction and diffusion capacitance associated with the carrier lifetime of the semiconductor device (Mynbaev & Scheiner, 2000). Herman *et al*. used an LED with a small active area and consequently low output power, and were able to modulate the device at frequencies up to 250 MHz. However, implementation of wide-field FD-FLIM calls for the use of LEDs with larger active areas and high average output power, which puts limits on achievable modulation bandwidths. The bandwidth for the large-active area, high power LEDs used in the present work (Luxeon III Star, Lumileds) was of the order of 40 MHz. A key question to be addressed in the current work is how useful such devices are for resolving lifetimes of biologically relevant fluorophores. Furthermore, we wish to establish what minimum lifetime differences can be resolved between features in the imaged object. Usually, lifetimes of 1 ns or less are considered to be below the limit of resolution at such relatively modest modulation frequencies.

Modulation frequency

In Fig. 1(a) and (b), sensitivity analyses are presented for the measurement of lifetime components. The rate of change of the phase shift $(\partial\phi/\partial\tau)\tau$ [Fig. 1(a)] and the demodulation $(\partial m/\partial\tau)\tau$ [Fig. 1(b)] of the signal are plotted as a function of modulation frequency. Curves are shown for lifetimes $\tau = 4$ ns and $\tau = 0.6$ ns. Dashed lines on the plots indicate the range of modulation frequencies used in the current work (between 10 and 40 MHz). The maximum modulation depth was around 30% at 40 MHz, and the modulation depth decreased significantly for higher frequencies. For measurements of the phase

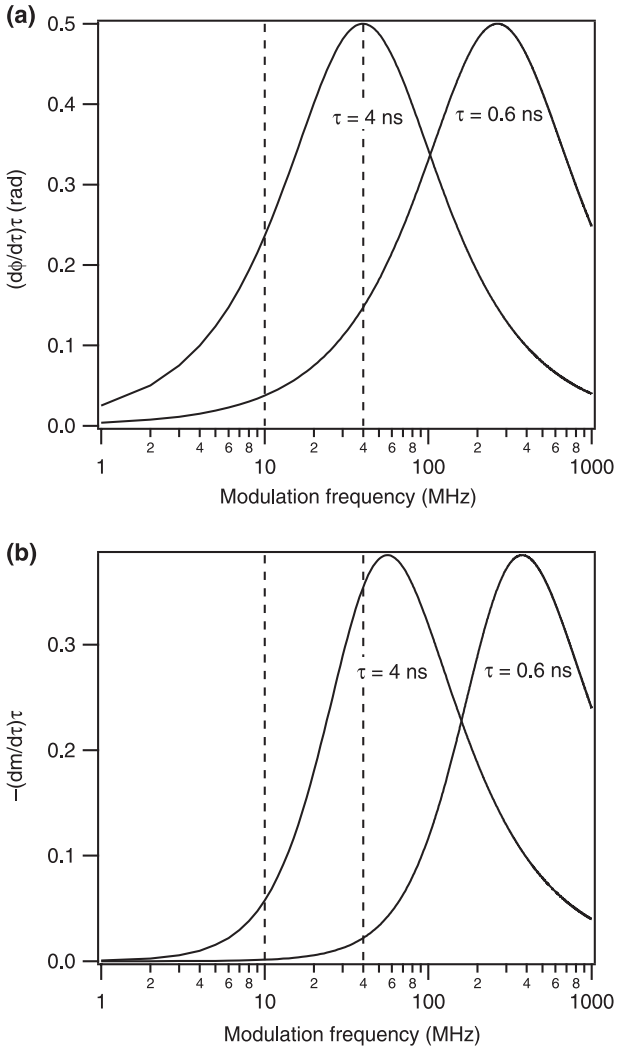

Fig. 1. Sensitivity of phase change (a) and modulation change (b) to fluorescence lifetime as a function of modulation frequency, for lifetimes $\tau = 4$ ns and $\tau = 0.6$ ns. Dashed lines indicate the bandwidth over which the LEDs were modulated in the present work.

lifetime, τ_ϕ, maximum theoretical sensitivities are achieved at frequencies:

$$\omega_{\text{opt}.\phi} = \frac{1}{\tau} \tag{5}$$

A modulation frequency of 40 MHz offers close to optimal sensitivity for measurements of phase lifetimes for τ near 4 ns. In contrast, the sensitivity for subnanosecond lifetimes is rather modest for modulation frequencies between 10 and 40 MHz. At $\tau = 0.6$ ns, the sensitivity peaks near 265 MHz, and thus appreciable measurement errors are expected for the short lifetime component.

Optimal frequencies for measurements of modulation lifetimes are given by:

$$\omega_{\text{opt}.m} = \frac{\sqrt{2}}{\tau} \tag{6}$$

corresponding to peak sensitivities for the $\tau = 4$ ns lifetime at 56 MHz, and for $\tau = 0.6$ ns at 375 MHz. At 40 MHz, a lifetime of 0.6 ns gives a demodulation of only 1.1% with respect to the excitation waveform, suggesting very limited sensitivity and significant susceptibility to system drifts, measurement noise and artefacts introduced by imprecise background subtraction. For a detailed discussion on sources of errors in time-resolved measurements see vandeVen *et al.* (2005).

The sensitivity analysis presented above is valid only in the case of infinite signal-to-noise ratios (SNRs). Philip & Carlsson (2003) deduce optimal modulation frequencies in the presence of noise and find that:

$$\omega_{\text{opt}.\phi} = \frac{0.7}{\tau}, \tag{7}$$

$$\omega_{\text{opt}.m} = \frac{1.4}{\tau} \tag{8}$$

This result suggests that the discrepancy between optimal modulation frequencies for phase and modulation lifetimes is even larger for finite signal-to-noise ratios. In the following sections, we explore these issues in detail and recommend strategies to maximize measurement fidelity.

Materials and methods

Frequency-domain FLIM microscopy system

Figure 2 shows a set-up for the system used in the present work. FLIM measurements were performed using an Olympus IX50 inverted microscope (Olympus UK, Southall, U.K.). Lenses used were a 10× (Olympus UPlanApo 0.4 NA/air) for the microchannel work and a 100× (Olympus UPlanSApo 1.4 NA/oil immersion) for the live cell work presented below. The FWHM of the PSF for the 100× lens system was measured to be around 750 nm, limited by the image intensifier. Sample illumination was provided by a 3 W LED with a peak emission

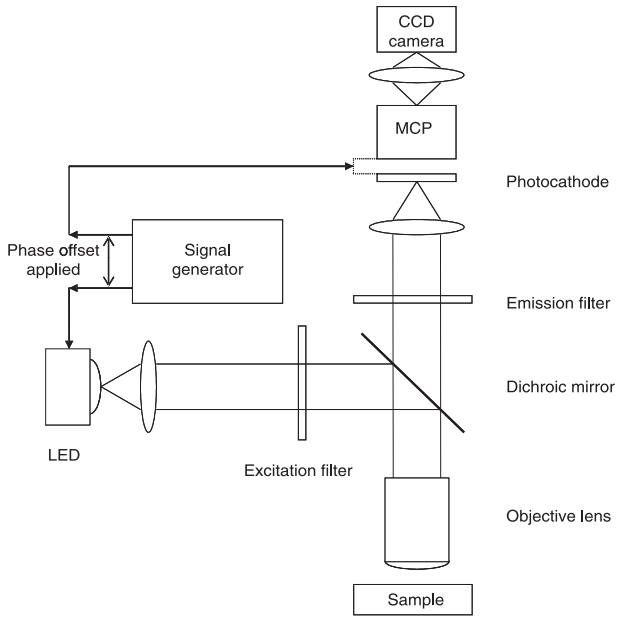

Fig. 2. Diagram illustrating the main components of the frequency domain FLIM setup. The voltage on the photocathode of the MCP intensifier is modulated at the desired frequency by the signal generator. The current to the LED is modulated at the same frequency, but with a well-defined phase offset. A series of images taken at different phase offsets allow determination of the fluorescence lifetime in every pixel of the image.

wavelength of 480 nm and a 40-nm bandwidth (Luxeon III star, Lumileds Lighting, U.S.A.). The system was configured for excitation of Rhodamine 6G dye solution and this configuration was used for all measurements presented in this paper, including application examples. Appropriate wavelengths for sample excitation and emission were selected using a 470–490 nm band-pass excitation filter, 505 nm dichroic mirror and 545–580 nm band-pass emission filter. Fluorescence emission was detected using a Gen II microchannel plate (MCP) intensifier (II18MD, Lambert Instruments, Netherlands) and a CCD camera (CCD-1300D, VDS Vosskuhler). The CCD was used in 2 × 2 binning mode (intensifier resolution limited) yielding an image of 640 × 512 pixels. The LED emission and intensifier gain were modulated at the same frequency using a signal generator (LIFA modulation signal generator, Lambert Instruments) that allowed a well-defined phase offset to be imposed between the LED and intensifier modulation waveforms. The intensifier's photocathode voltage was modulated, and the MCP voltage was kept constant. A series of images taken at different phase offsets allowed the lifetime in each pixel of the image to be calculated. The phase shift and demodulation of the fluorescence emission at angular frequency, ω, were determined on a pixel-by-pixel basis by fitting the fluorescence signal from the different phases to a sine function. The amplitude and dc offset of the modulated LED intensity were kept constant between measurements of the reference and sample solutions.

Fitting algorithm

Software was written in IDL (Interactive Data Language, Research Systems Incorporated) to extract lifetimes from the fitted sine functions in each pixel. Phase shift, amplitude and dc offset were obtained from the waveforms by fitting a function of the form:

$$f = \theta_1 + \theta_2 \cos(\varphi - \theta_3) \tag{9}$$

to the experimental data. By rewriting the cosine term, Eq. 9 can be linearized in cos(φ) and sin(φ), respectively:

$$\begin{aligned} f &= \theta_1 + \theta_2 \cos(\theta_3)\cos(\varphi) + \theta_2 \sin(\theta_3)\sin(\varphi) \\ &= a_1 + a_2 \cos(\varphi) + a_3 \sin(\varphi) \end{aligned} \tag{10}$$

For Gauss-Markov conditions and normally distributed errors, the least squares estimate corresponds to the maximum likelihood estimate of the parameters a_i. Since Eq. 10 is linear in terms of cos(φ) and sin(φ) the least squares estimate can be obtained analytically from:

$$\underline{a}_{LS} = \left\lfloor (X^T X)^{-1} X^T \right\rfloor \underline{f} \tag{11}$$

where X is given by:

$$X = \begin{pmatrix} 1 & \cos(\varphi^{[1]}) & \sin(\varphi^{[1]}) \\ 1 & \cos(\varphi^{[2]}) & \sin(\varphi^{[2]}) \\ & \vdots & \\ 1 & \cos(\varphi^{[N]}) & \sin(\varphi^{[N]}) \end{pmatrix} \tag{12}$$

where the superscripts 1 to N refer to the phase step number.

Since X is the same for every pixel this represents an efficient method of fitting the modulation data as only one matrix multiplication is required for each pixel. The demodulation and phase shift are determined from the parameters a_i using the expressions:

$$m = \frac{\sqrt{a_2^2 + a_3^2}}{a_1} \tag{13}$$

and

$$\phi = \arctan\left(\frac{a_3}{a_2}\right) \tag{14}$$

The calculation of lifetimes from fluorescence images (640 × 512 pixels) obtained at 12 phase positions was accomplished in under 4 s on a 2 GHz Pentium PC with 512 MB of RAM.

An alternative to the above approach is to operate in the frequency domain after Fourier transformation of the data (Robert *et al.*, 1994). The Fourier transformation approach is equivalent to the method described above, however, it requires the use of equidistant phase steps (Boddeke, 1998). The method adopted in this work will permit us to explore the use of non-equidistant phase steps in the future and to test whether this provides a means to record at faster rates with improved sensitivity.

Note that although a_1, a_2 and a_3 are unbiased estimators, the nonlinear operation in Eq. 13 leads to bias in m. Because of the square root term in Eq. 4 even a small bias in m can lead to relatively large errors in the mean modulation lifetime $<\tau_m>$. In order to avoid bias in $<\tau_m>$, averaging is performed on unbiased estimators rather than simply averaging τ_m. This bias can introduce significant errors at short lifetimes and low signal-to-noise ratios and all modulation data presented here was therefore evaluated using such methods. A discussion of the statistical methods applied is beyond the scope of the present paper but will be dealt with in detail in a forthcoming publication.

Calibration of system

The FLIM imaging system was calibrated using a series of reference solutions, which were prepared according to the protocol detailed by Hanley. The solutions contained Rhodamine 6G dye at 1 μM concentration in water with an ionic strength of 0.2 M. The fluorescence lifetimes were varied by adding potassium iodide (KI) in concentrations ranging from 0.000 to 0.200 M, whilst maintaining the ionic strength by the addition of potassium chloride (KCl). Iodide quenching of Rhodamine 6G, Rh6G, is known to produce mono-exponential decay standards with variable lifetimes (Hanley *et al.*, 2001; Harris & Lytle, 1977). Solutions were pipetted into black, glass bottomed multiwell dishes, which were enclosed to prevent dilution changes by solvent evaporation. Care was taken to avoid bleaching of fluorophores at all times.

For comparisons, we performed independent fluorescence lifetime measurements using other methodologies. These included time-correlated single-photon counting (TCSPC) performed using output from a pulse picked Ti : Sa laser and two-photon excitation of Rh6G at 980 nm (Becker and Hickl SPC830 fitted to a Leica SP2 microscope frame). The fluorescence was short pass filtered (< 700 nm) before detection on a fast photomultiplier tube.

A second set of fluorescence-lifetime measurements was performed in the frequency domain using the second harmonic (λ = 532 nm) of a cw Nd:YAG laser for single-photon fluorescence excitation. The laser-beam intensity was modulated at 30 MHz with an AOM. The fluorescence was detected with a microchannel-plate (MCP) photomultiplier tube, and the laser intensity was monitored on a photodiode. The photodiode signal was filtered with a bandpass filter centred at 30 MHz to reduce out-of-band interference. The phase difference between the photomultiplier and the photodiode signals was measured with a lock-in amplifier (Stanford Research Systems SR830). The fluorescence lifetime was determined from Eq. 3 using elastic scattering from frosted glass as the reference signal. In a third set of experiments, the temporal decay of fluorescence was measured after excitation by the second harmonic of a regeneratively amplified Nd:YAG laser with a

Table 1. Lifetimes of Rhodamine 6G solutions.

Solution	[KI] M	τ_ϕ (ns)	τ_m (ns)	TCSPC (ns)	AOM/Lock-in (ns)	MCP/PMT TD (ns)	Hanley *et al.* (2001) (ns)
1	0	4.06 ± 0.17	4.09 ± 0.17	N/A	4.08	3.97	4.08 ± 0.02
2	0.005	3.61 ± 0.15	3.58 ± 0.17	3.45	3.66	3.54	3.60 ± 0.01
3	0.03	2.27 ± 0.09	2.26 ± 0.15	2.32	2.38	2.18	2.26 ± 0.02
4	0.05	1.75 ± 0.06	1.71 ± 0.15	1.80	1.84	1.65	1.67 ± 0.02
5	0.1	1.11 ± 0.04	1.12 ± 0.16	1.14	1.15	1.10	1.05 ± 0.04
6	0.2	0.69 ± 0.04	0.81 ± 0.21	0.65	N/A	0.61	0.61 ± 0.03

pulse duration of approximately 70 ps. The fluorescence signal was detected with an MCP photomultiplier tube and recorded on a digital oscilloscope with 6 GHz bandwidth. The fluorescence traces were fitted to a single-exponential decay convolved with the instrument response function, which was measured using elastic scattering. Details on this system and its calibration are found in Settersten *et al.* (2002).

Finally, the results of all measurements were compared to the lifetimes reported by Hanley *et al.* (2001) who used an AOM based widefield FLIM system at 58 MHz modulation frequency. Results of all measurements are given in Table 1 and will be discussed in detail in a later section.

Susceptibility of phase and modulation lifetimes to noise

To assess the effect of image noise on the calculated lifetimes, simulations were performed on computer generated images with varying degrees of normally distributed noise superimposed. Lifetimes were assumed to be uniformly distributed and for each lifetime, a series of 12 signal images was generated, corresponding to the number of phase steps used in the experiments. The reference lifetime was also chosen to be 4.08 ns in order to mimic the experiments. For the reference signal, a dc level of $A_{\text{ref}} = 19\,000$ counts, and a modulation amplitude of $a_{\text{ref}} = 7500$ counts were chosen to generate signal images that mimicked the signals in the Rhodamine 6G reference measurements at $\tau = 4.08$ ns. Next a set of corresponding sample images were generated for the range of sample lifetimes investigated. Again τ_{spl} was assumed to be homogeneously distributed over the image. For the sample images a dc level of $A_{\text{spl}} = 19\,000$ was chosen. The phase shift and demodulation with respect to the reference image were calculated, and corresponding signal images were generated at each of the phase positions. Finally, random Gaussian noise was superimposed on the reference and signal images with signal-to-noise ratios ranging from 20 to 500. The signal-to-noise ratio is defined as the ratio of the mean signals, A_{spl} and A_{ref}, to the standard deviation of the noise amplitude spectrum. Fluorescence lifetimes were determined from the simulated reference and sample images using the same software that was used for all of the experimental data.

Smallest resolvable lifetime differences

We explore through simulations the ability of the system to provide contrast between variably sized objects with differing lifetimes within images. Hanley *et al.* differentiate between the capability of FLIM to distinguish between inter and intraimage lifetime differences, and they show that errors associated with the former can be 1–2 orders of magnitude larger. For many applications, the ability to provide contrast between regions of differing lifetimes is the most important criterion. The smallest resolvable lifetimes within an image are determined by the noise distributions of component lifetimes, which result from measurement noise, i.e. photon and detector noise. Instrument drift or background level changes cause systematic deviations which are likely to be of greater significance between acquisitions than for intraimage feature discrimination.

Human vision is remarkably sensitive to patterns in images even in the presence of significant noise, and criteria based on visual discrimination of lifetimes are necessarily subjective. An objective quantification method is required to assess measurement fidelity. We perform a Student's *t*-test, which assumes normally distributed data, using two regions to see whether the mean lifetimes are different. If the means of the two regions are denoted by $<\tau_1>$ and $<\tau_2>$, and the number of pixels in each region are denoted by n_1 and n_2, respectively, then the expression for the Student's *t*-test is:

$$t = \frac{|<\tau_1> - <\tau_2>|}{s} \sqrt{\frac{n_1 n_2}{n_1 + n_2}} \tag{15}$$

where *s* is the pooled standard deviation,

$$s = \sqrt{\frac{\sum_{i=1}^{n_1} (\tau_{1,i} - <\tau_1>)^2 + \sum_{j=1}^{n_2} (\tau_{2,j} - <\tau_2>)^2}{n_1 + n_2 - 2}}. \tag{16}$$

At 99% confidence level $<\tau_1>$ and $<\tau_2>$ are significantly different if $t > 2.6$. An important case to consider is the discrimination of a region with a lifetime $<\tau_2>$ embedded in a much larger region with a lifetime $<\tau_1>$. We model this situation for different SNRs by estimating minimum resolvable lifetime differences (99% confidence) for large values of n_1 and varying n_2.

Results and discussion

Quenched Rhodamine 6G solutions

The results from the calibration of the system with iodide-quenched Rhodamine 6G solutions are presented in Table 1. The table includes data from 4 independently performed measurements using the alternative techniques described earlier. Errors correspond to one standard deviation, calculated from the distribution of lifetimes in one image. The lifetime of the reference, which was a Rhodamine 6G solution with no iodide quenching, was assumed to be 4.08 ns (Lakowicz & Berndt, 1991; Hanley *et al.*, 2001; Harris & Lytle, 1977). The 3rd and 4th columns in Table 1 demonstrate that there is good agreement between the modulation lifetime estimates with the (much more precise) phase lifetimes even down to the lowest measured lifetimes. This agreement is somewhat surprising considering the very low sensitivity of the demodulation measurement (see Fig. 1b) at the modulation bandwidths of the LEDs. At a lifetime of 0.6 ns demodulations are of order 1%, and small dc drifts (which could result from bleaching or electronic drifts) will dramatically impact the demodulation measurement fidelity, however, phase measurements remain relatively robust (see subsequent discussion for more detailed comments on such effects). For $\tau = 0.6$ ns, the relative errors in the modulation lifetime measurements are around 25% as opposed to only 6% for the corresponding phase shift measurement. Note that the phase and modulation measurements were performed using the same camera settings with an exposure time of 120 ms. The exposure times for the other frequency domain techniques referenced here are unavailable. Measurement fidelity can be improved with longer collection times but care must be taken to avoid any bleaching of the sample which would significantly bias the demodulation lifetimes.

Figure 3 shows comparisons between the LED FLIM phase lifetime measurements and the 4 other sets of lifetime measurements. The data are shown in the form of Stern-Vollmer plots such that linear fits through the data points can

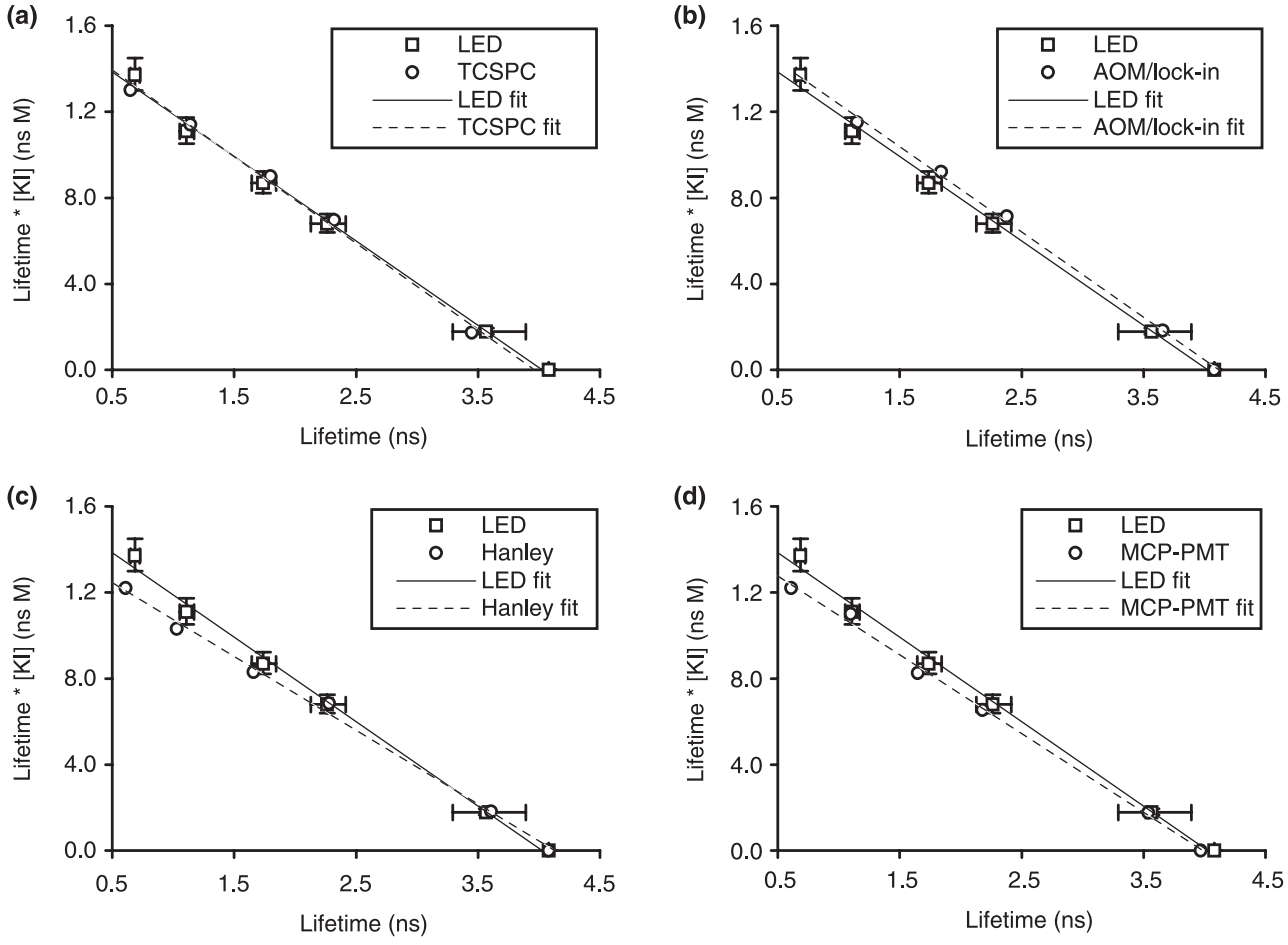

Fig. 3. Stern-Vollmer plots for I^- quenched solutions of Rhodamine 6G comparing 5 independent lifetime measurement methods. Comparison of FD-LED FLIM with (a) Time Correlated Single photon counting (TCSPC) experiments, (b) FD FLIM obtained using an acousto optic modulator and lock-in detection, (c) FD FLIM experiments using an AOM modulated Ar-ion laser and rf-modulated intensified CCD detection and (d) picosecond excitation and fast gated detection in the time domain. The fits shown are linear fits through the data, as predicted by a Stern-Vollmer model.

be performed. The plots presented are a variation of the standard Stern-Vollmer plot often presented in the literature (see, e.g. Hanley *et al.*, 2001) where $1/\tau$ is plotted against quencher concentration. The advantage of the present form is that error bars will cluster more closely around the fit lines, visually reflecting the goodness of fit through the data in a clearer way than in the conventional plot, where the size of error bars are unevenly distributed due to the $1/\tau$ term.

In general, the agreement between the individual measurement techniques, which were carried out independently in several laboratories, is excellent, and the maximum discrepancy in lifetimes is around 100 ps. This agreement demonstrates the robustness of using quenched Rhodamine solutions as lifetime standards. Note that the analysis presented here does not take into account iodide concentration errors arising from inaccuracies in the sample preparation. Temperature variations may also contribute to the discrepancies since the iodide quenching rate is to some extent temperature dependent. Another possible error in the FD-FLIM measurements is the lifetime of the unquenched Rhodamine solution, which was used as the reference sample and assumed to have a lifetime of 4.08 ns. Even small deviations from this value would have effects on the slope on the graphs shown in Fig. 3.

Susceptibility to noise

Figure 4 shows results from the simulated evaluation of phase and modulation lifetimes with added noise for assumed lifetimes of 4.0 ns (top row) and 0.6 ns (bottom row). The simulations were performed for modulation frequencies of 40 MHz (left column) and 20 MHz (right column). The error bars correspond to one standard deviation of the lifetimes for a sample of size $n = 100\,000$. The significant asymmetry of the error bars for τ_m arise from the bias that was discussed earlier. At 40 MHz modulation and a true lifetime of 4 ns, there is good correspondence between estimated and true lifetimes even at low SNRs, and the precision is similar for τ_ϕ and τ_m. For the 0.6 ns lifetime measured at 40 MHz, however, standard deviations are about 3 times larger for τ_m than for τ_ϕ. Lifetimes as large as 2 ns are estimated for a significant number of pixels.

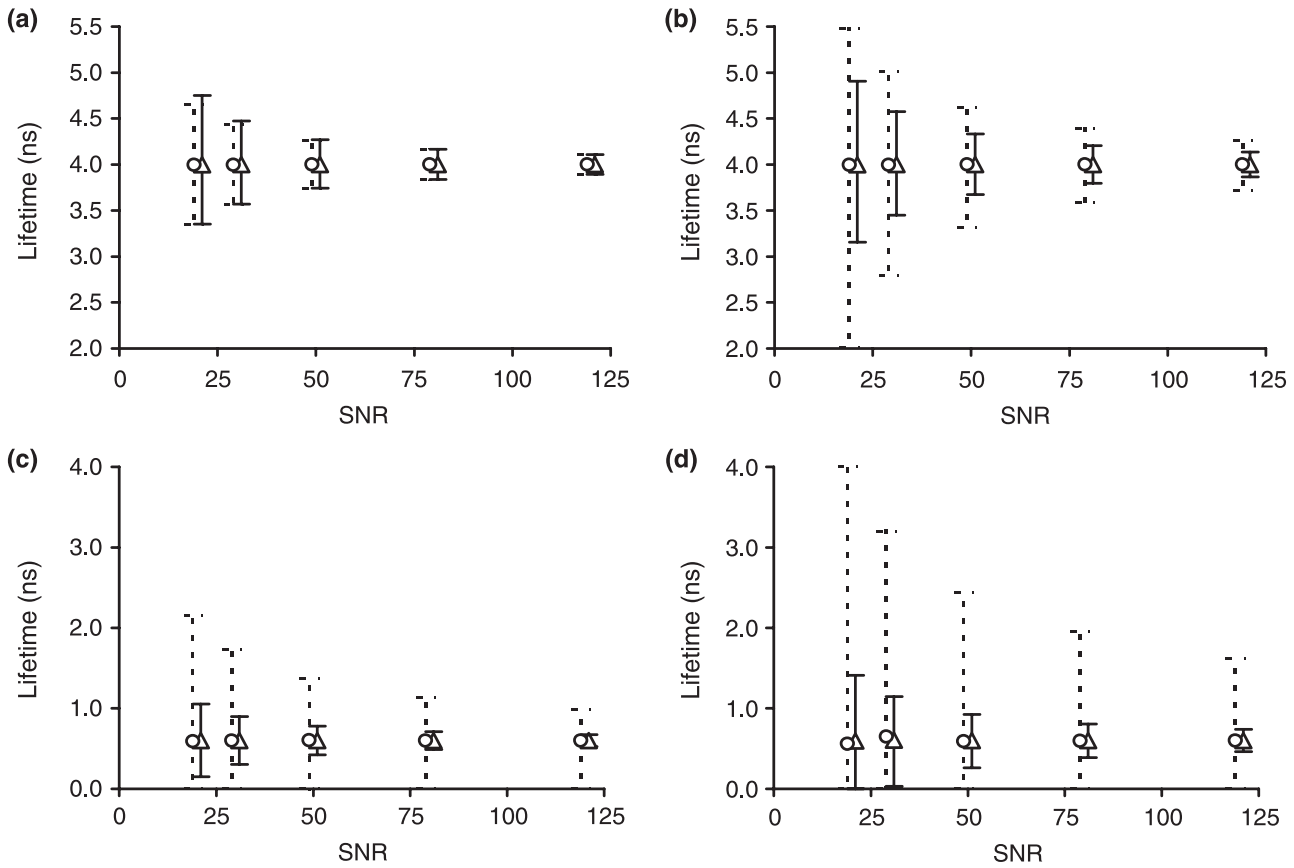

Fig. 4. Modelled variation of phase and modulation lifetimes as a function of signal-to-noise ratio (SNR). Data modelled for sample lifetimes of 4.0 and 0.6 ns, which are measured with modulation frequencies of 20 and 40 MHz: (a) Modelled data for a sample lifetime of 4.0 ns measured with a modulation frequency of 40 MHz, (b) 4.0 ns sample and 20 MHz modulation frequency, (c) 0.6 ns sample and 40 MHz modulation frequency and (d) 0.6 ns sample and 20 MHz modulation frequency. In all cases the circles with dashed error bars represent modulation lifetimes and the triangles with solid error bars represent phase lifetimes.

There are also a number of pixels that lead to a negative argument in Eq. 4, corresponding to a nonphysical situation for which lifetimes could not be evaluated. At 20 MHz modulation frequency and $\tau = 4$ ns, the precisions are worse for τ_m than for τ_ϕ by a factor of around 1.5, although the estimated mean lifetimes are still surprisingly accurate at this low modulation frequency. For the 0.6 ns lifetime simulation, the precision in τ_m is unacceptable for all signal-to-noise-ratios studied with lifetimes between individual pixels varying by a factor 6 or more.

Two conclusions can be drawn from this analysis: Firstly, phase lifetime measurements are accurate even at the relatively low modulation frequencies of the high brightness, large area LEDs. Lifetimes as short as 1 ns can be confidently evaluated from the phase lifetime measurements even at $\upsilon = 20$ MHz, although the theoretical optimum lies at 160 MHz for $\tau = 1$ ns. Secondly, the mean modulation lifetimes could be confidently measured for the large sample sizes considered here. However, the growing imprecision associated with decreasing SNRs and modulation frequencies may limit the usefulness of modulation lifetime measurements in practical situations. Note that the evaluation of τ_m requires the use of bias corrections, without which the systematic overprediction of evaluated lifetimes can be larger than the true lifetime by as much as a factor of 4 (data not shown).

Susceptibility to DC offset

An important consequence of the low demodulation values for small lifetimes is the susceptibility of τ_m measurements to DC offset drifts. When subns lifetimes are measured with low modulation frequencies, the demodulation is very small, and a drift of fractions of a percent in the dc offset can cause very significant errors in τ_m. In contrast, the phase lifetimes remain essentially unaffected. Calculations were performed in order to systematically study the effects of dc offset on modulation lifetime measurements, and the results are shown in Fig. 5. All calculations were done using a modulation frequency of 40 MHz. The figure shows a plot of the evaluated modulation lifetime as a function of the true lifetime (x-axis) for offsets ranging from 100% (true dc-offset) to 95%. The phase lifetime is indistinguishable from the true lifetime. The offset errors cause shifts of τ_m which above 2 ns approach a nearly constant value of around 100 ps per percent of change in the offset value. For small lifetimes, the effect is dramatic. For example, for a true lifetime of 0.5 ns an offset error of only 2% causes τ_m to nearly double, corresponding to an error of 100%.

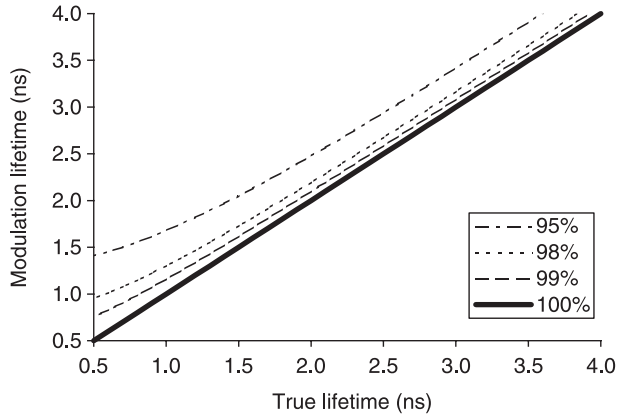

Fig. 5. Sensitivity analysis of modulation lifetime estimates to DC offset variations at 40 MHz modulation frequency. Modulation lifetimes are plotted against true lifetimes (from which phase lifetimes were indistinguishable).

Accurate background subtraction is therefore essential to minimize systematic errors in modulation lifetimes. Such errors may result from changes in ambient conditions, image persistence effects (e.g. due to finite phosphor decay times), and photobleaching. The latter effect must be borne in mind when increasing exposure times to maximize signal-to-noise ratios for samples with short fluorescence lifetimes.

For samples with subns fluorescence lifetimes, we observed a systematic increase in measured values of τ_m for relatively long exposure times. The measurements presented here were therefore made at a constant exposure time for which the effects of photobleaching were minor. A disadvantage of this approach is that the signal-to-noise ratios are lower for samples with shorter lifetimes. van Munster *et al.* (2004) suggest a method for mitigating some of the effects of photobleaching through a permutation of the recording order of the different phases, but this approach was not used here.

Large errors may also be introduced through uncertainty in the reference lifetime. Hanley *et al.* (2001) report on a calibration method for dye solutions exhibiting single exponential lifetime decays that does not require a *priori* knowledge of a reference lifetime. In their approach, the reference lifetime is determined by comparing phase and modulation lifetimes for a series of samples with a range of lifetimes. An incorrectly assumed reference lifetime leads to systematic differences between phase and modulation lifetimes. A plot of τ_ϕ against τ_m will only converge to a straight line with a slope of 1 if a correct reference lifetime is used. Whilst self calibrating, the method requires an excellent measurement precision, which is unlikely to be obtained at the low modulation frequencies in the present experiments.

Resolvable lifetime differences

Results from simulations are shown in Fig. 6 to assess the systems capability of measuring lifetime differences between different image objects. It shows images containing 5 adjacent regions ($n_i = 8000$) with differing lifetimes. Noise was added to the data in the same manner as previously described, to obtain SNRs ranging from 20 to 500. The histograms of lifetimes for all data points in all five regions are shown below each image. The nominal mean lifetimes in the five squares were 4.0, 4.1, 4.2, 4.3 and 4.4 ns. At SNR = 20, the histograms are strongly blended into each other even though it is still

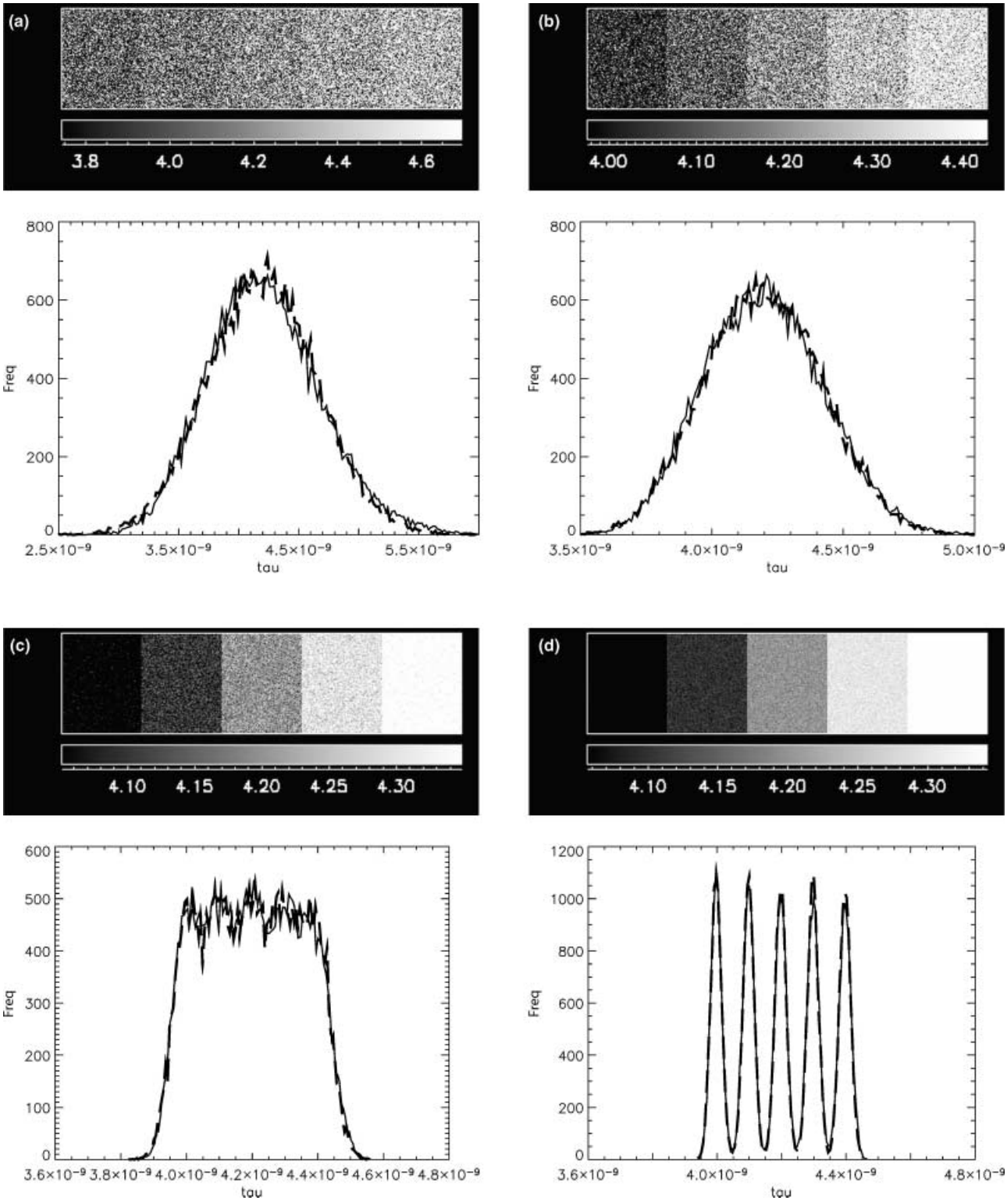

Fig. 6. Simulations to establish mininimum resolvable lifetime differences between 5 adjacent image regions ($n_i = 8000$ pixels), each with differing lifetimes. The lifetime between individual regions increases by 100 ps steps from left to right, increasing from 4.0 to 4.5 ns. The signal-to-noise ratios (SNR) correspond to 20, 50, 200, and 500 for regions (a) to (d), respectively. Below each simulated image a histogram is plotted of the lifetime distributions based on statistics of the entire image sample ($n = 40\,000$ pixels). On the histogram, solid lines correspond to τ_ϕ and dashed lines to τ_m.

just possible to discern the different image regions by eye. For a SNR of 50 the image regions are clearly discernible, whereas on the histograms no structure is visible. The histograms do not reflect the fact that in the images shown pixels with similar lifetimes are clustered in spatially distinct regions. One is clearly able to differentiate between individual lifetime regions well before clearly separated and discernible peaks appear on corresponding histograms. Only at SNR of over 200, does one begins to see a separation between individual peaks in the histograms, indicating that the precision of the measurement now exceeds the lifetime difference between the individual regions (100 ps). In other words, for clearly separated peaks, each individual pixel can be assigned to its corresponding lifetime class.

Note that the constraints on measurement precision for differentiating between two regions within different images (*inter* image resolution) are significantly greater than for two regions within the same image (*intra* image resolution).

Additional simulations were used to evaluate *intra* image resolution requirements. Figure 7 shows the minimum resolvable lifetime difference for a small object that is embedded in a larger region of differing lifetime. The resolution criterion is set according to a *t*-test analysis at the 99% confidence level. Simulated data were used where n_1 was the number of pixels in the background region, $n_1 = 10\,000$, and the minimum resolvable lifetime difference is plotted as function of n_2, i.e. the number of pixels in a smaller subregion. Data are shown for SNRs of 20, 50 and 100, and the nominal mean lifetime of the background ($\bar{\tau}_1$) was 4.0 ns. The minimum resolvable lifetimes show a nonlinear dependence on the size of the smaller feature. For an image feature of size 100 pixels (e.g. 10×10), a SNR of 20 (50) results in a minimum resolvable lifetime difference of 100 ps (50 ps). The same analysis was done for background regions with lifetimes of 1.0, 2.0 and 3.0 ns. The results showed that the minimum resolvable lifetimes were shifted to slightly smaller values: at SNR = 50, the 100 pixel resolvable lifetimes were about 20, 25, and 35 ps, respectively (data not shown). When performing lifetime imaging in practical situations, regions of interest are normally determined by a *priori* information, e.g. one expects protein binding to occur in certain structures within the cell. These regions of interest can be delineated in the lifetime image by colocalization of structures seen in the normal microscope image or the fluorescence intensity image.

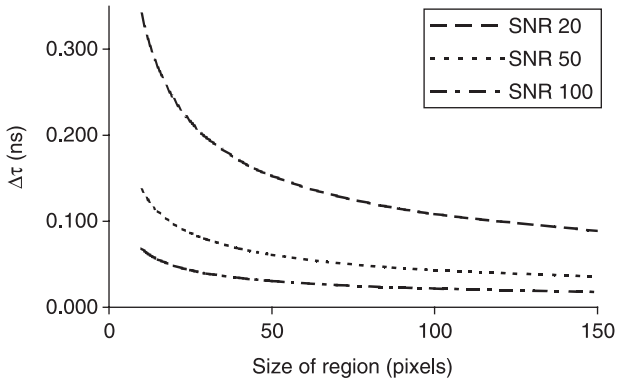

Fig. 7. Minimum resolvable lifetime differences ($\Delta\tau$) for detection of a small image feature embedded in a larger region ($n_1 = 10\,000$ pixels) with a different lifetime. The results are shown for three different SNRs and are stated at 99% confidence level according to a Student's *t*-test. Data are shown for a 4 ns lifetime and a 40 MHz modulation frequency.

Applications

In this section, some practical applications of the FD-FLIM system illustrate its potential. We first consider fluorescence lifetime measurements in a microchannel flow (Benninger *et al.*, 2005). Figure 8(a) shows a fluorescence intensity image in a system consisting of two flow channels merging into a single channel (dimensions 500 μm across the single channel,

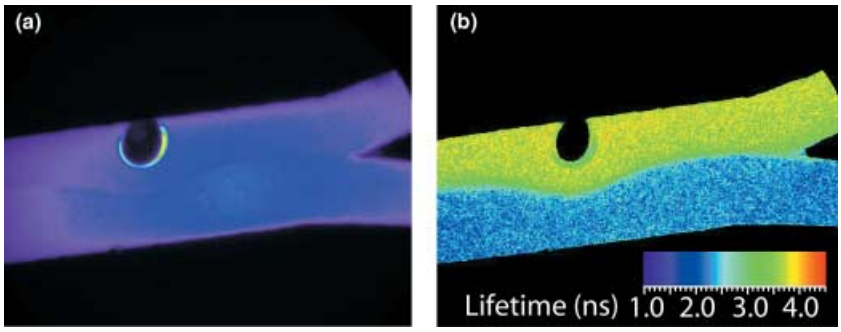

Fig. 8. (a) Fluorescence image of two streams of dye solution merging into a single channel (channel width 500 μm). The top channel on the right contains Rhodamine 6G dye in KCl, and the bottom channel contains Rhodamine 6G in KI solution. Flow is from right to left. The circular feature is an air bubble trapped on the channel wall. (b) Corresponding lifetime image. A clear contrast is obtained between the different flow streams and the mixing layer is clearly defined. Lifetimes vary from around 4 ns in the top flow, to around 2 ns in the lower flow, where the Rhodamine lifetime is strongly quenched by the iodide ions. A threshold was applied to the raw data to remove background pixels in regions outside the channel. Measurements shown were performed using 12 phase steps with individual collection times of 30 ms.

depth 100 μm). The top channel on the right contains Rhodamine 6G in KCl and the bottom contains Rhodamine 6G in KI and flow is from right to left. The dye concentrations of the two streams were adjusted to yield similar intensities thus offering very low contrast between the two fluid streams. The flow was gravity driven and controlled by adjusting the height of two large dye dispensing reservoirs. The flow speeds were approximately 10^{-3} ms^{-1}) with a corresponding Reynolds number of order Re = 0.5. The black circular region on the top wall near the middle of the channel is a trapped air bubble. In Fig. 8(b), the corresponding fluorescence lifetime image is shown. This example demonstrates that FLIM is capable of providing excellent contrast in situations where intensity-based measurements fail. The lifetime image shows a very sharp boundary between the two fluid streams. The gradient across this boundary layer gradually decreases with distance as the two streams mix by diffusion. The device allows cross diffusion of ions to be studied (Elder *et al.* 2005) and has potential for determination of molecular mixing scales. For the data shown here, fluorescence images were acquired at 12 phase angles using a 30 ms integration time for each phase. Fast camera technology with additional amplification (e.g. electron multiplication gain cameras in combination with intensifiers) could significantly increase the speed of these measurements. Lifetime images could be acquired in as little as 100 ms, permitting dynamic information to be captured, which is an advantage for *in vivo* applications.

We are currently investigating the use of microchannel devices for the measurement of polymer conformational dynamics. We have used the system to study conformational changes in fluorescently labelled amphiphilic polymers (poly-L-lysine iso-phthalamide), which have been synthesized as tumour markers and drug delivery vehicles (Eccleston *et al.* 2004; Dai *et al.* 2006). The polymer backbone contains hydrophobic and hydrophilic parts. The polymer adopts an extended conformation at low degrees of ionization and a compact globular structure, or hypercoil, at high degrees of ionization. This environmentally dependent conformational change was investigated both *in vitro* and *in vivo* using our FD-FLIM system (only *in vitro* data shown here). The polymer contained cyanine (cy-3) fluorophores, and the hypercoiling was accompanied by marked reductions in the fluorescence lifetime of the fluorophore. The rate of self-quenching increases as the polymer structure collapses and the fluorophores come into closer proximity with one another. *In vitro* experiments were performed in multiwell plates that were placed on the FLIM microscope to measure lifetime changes as a function of acidification. The results are shown in Fig. 9, which displays cy-3 lifetimes at different pH for 4 different polymer concentration values (averaged over $n = 1000$ pixels). Upon acidification down to pH 4.0 from a pH of 7.0 a lifetime change from 1.28 ns down to 490 ps occurs in the cy3-polydye complex at concentration of 0.5 mg mL^{-1}. Control solutions of pure cy3 showed no corresponding change in lifetime (data shown in inset). Note that the conjugated dyes exhibit a longer lifetime (~1.5 ns) compared to the free dye

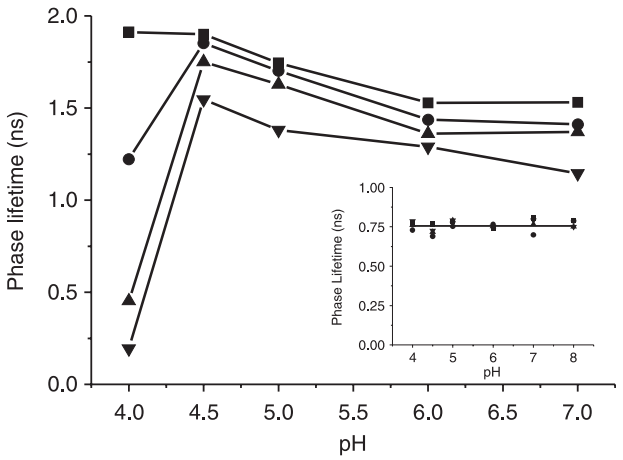

Fig. 9. Lifetime behaviour of cy3-polydye complex as a function of pH and concentration. The polydye concentrations are 2.0 (■), 1.0 (●), 0.5 (▲), and 0.05 (▼) mg mL^{-1}, respectively. The sharp drop in lifetimes around pH = 4.5 is concomitant with a collapse of the polymer structure from an extended structure to a hypercoiled conformation, with associated increased levels of self-quenching between the cy-3 fluorophores. At increasing polymer concentrations in solution, the onset of aggregate formation is visible. The formation of rigid structures hinders the full collapse of the molecules, and the fluorescence lifetimes increase (squares). The inset shows the lifetime of free (unbound) cy3 which is unaffected by pH.

(~0.75 ns), which is a manifestation of the reduced motility of the fluorophores when attached to the macromolecular structure and the increasing degree of protection from quenching species in solution (e.g. O_2). The effect is dependent on polymer concentration. For high degrees of polymer loading, the lifetime decrease is not observed. This result is indicative of the formation of aggregates at high polymer concentrations, leading to the formation of macroscopic, rigid structures that prevent the full collapse of the macromolecules and the associated fluorophore self-quenching. The structures provide increased protection against collisions with quencher species in solution. In previous papers, it was shown that these polymers have the ability of entering cells via pH mediated membrane rupture and endocytosis (Eccleston *et al.*, 2000). The environmental changes encountered by the polymer following cellular uptake permit the design of bioresponsive macromolecules.

An example of a live cell application of the FD-FLIM system is shown in Fig. 10. The images show the uptake behaviour of Doxorubicin, a DNA-intercalating drug, widely used in chemotherapy as an anticancer agent (Kiyomiya *et al.*, 1999). The molecule has a strong affinity for binding to DNA molecules through intercalation between adjacent base pairs. The intercalation inhibits DNA transcription and thus proliferation of cancerous cells. Doxorubicin contains several aromatic rings and is strongly fluorescing upon excitation near 473 nm and its emission peaks near 595 nm. Figure. 10(a,d) show fluorescence images of doxorubicin distributions inside live Hela cells incubated for 24 h with medium containing doxorubicin at

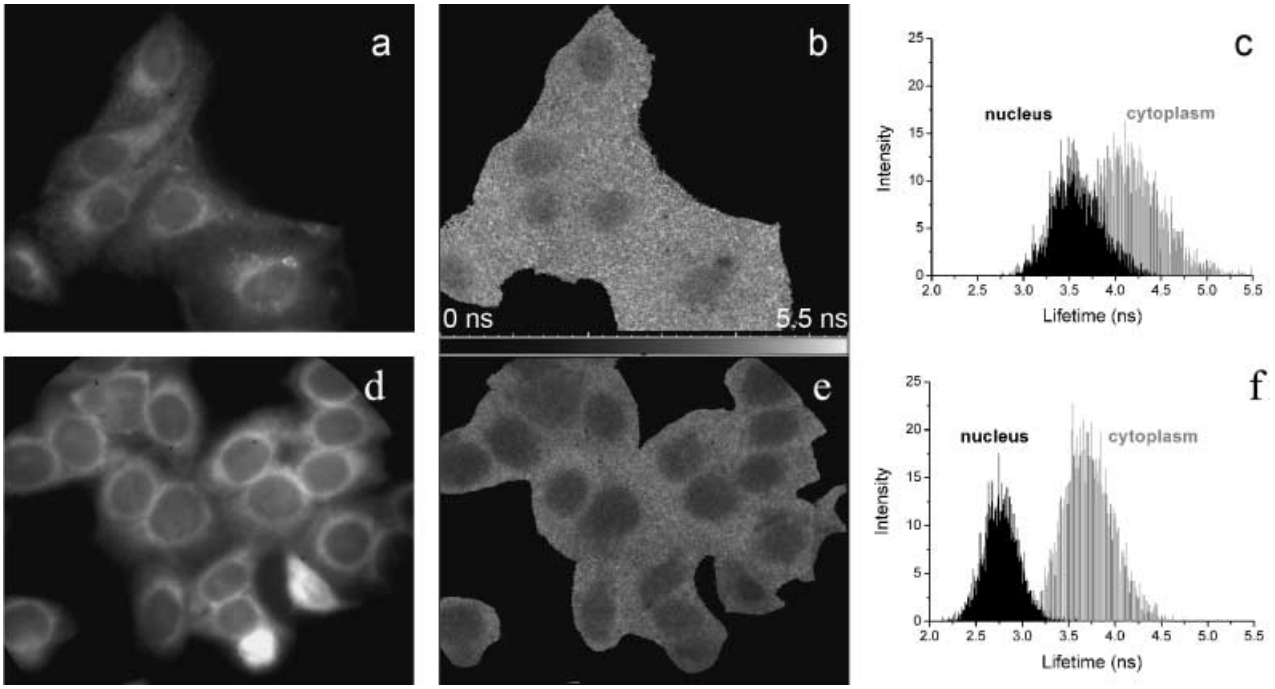

Fig. 10. Fluorescence intensity, lifetime images and corresponding lifetime histograms of doxorubicin in Hela cells (from left to right, respectively). Hela cells were incubated with doxorubicin at concentrations of 0.01 mg mL^{-1} (a,b,c) and 0.05 mg mL^{-1} (d,e,f) for 24 h prior to lifetime imaging. The lifetime distributions are clearly different in the cytosolic and nuclear domains. There is also a marked shift of lifetimes to shorter values as polymer concentrations are increased. The field of view is 160×128 μm^2. A threshold was applied to intensity data prior to calculation of lifetimes to remove data from low intensity pixels. Measurements shown were performed using 12 phase steps with individual collection times of 200 ms.

concentrations of 0.01 mg mL^{-1} and 0.05 mg mL^{-1}. Figure. 10(b,e) show corresponding lifetime images and Fig. 10(c,f) show histograms of the corresponding lifetime distributions. Doxorubicin is transported into the cell via endocytosis and attaches to macromolecular structures inside the cell leading to an increased lifetime relative to free doxorubicin in aqueous solution because of increasing protection against dissolved quencher species such as O_2. The doxorubicin is efficiently translocated into the nucleus by the cell. From Fig. 10(a)–(c) it is seen that the lifetime distributions in the cytosolic and nuclear domains differ significantly (4 ns vs. 3.5 ns) offering diagnostic information beyond that of purely intensity based measurements. As intercalation in the DNA reaches saturation, the concentration of free doxorubicin inside the nuclear domain increases, leading to an increased degree of self-quenching, and thus causing a shortening of the effective lifetimes. The different pH levels in the cytosol and the nucleus may be a further factor in the lifetime decrease of the molecule. Figures 10(d)–10(f) show the same information for a cell culture incubated with a higher concentration of doxorubicin (0.05 mg mL^{-1}) and the lifetime distributions for both cytosolic and nuclear doxorubicin have shifted to shorter lifetime values by a significant amount. The cytosolic component has shifted from 4 ns to 3.75 ns, whereas the nuclear component has reduced from 3.5 to only 2.75 ns, evidence of increased degrees of concentration dependent self quenching.

Conclusions

The results presented in this paper show that LED based frequency-domain FLIM provides a feasible alternative to established methodologies, such as time correlated single photon counting or time gated detection. The advantages of the system include the very low cost of the light sources and the significantly reduced complexity of the experimental set-up. The acquisition speeds permit application in dynamic systems, such as living cells, or microfluidic devices. This development has been made possible through the advent of very high brightness, large area LED devices, whose illumination properties ideally match wide field fluorescence microscopy systems. The availability of a large range of colours, the low cost and robustness allow versatile use for a multitude of applications. The downside is their relatively low modulation bandwidth that is limited by the capacitance of these devices. We have conducted experiments and simulations to assess the capabilities of such a device emitting near 470 nm, with a modulation bandwidth of approximately 40 MHz. Calibration measurements in Rhodamine 6G dye solutions demonstrated that despite this low modulation bandwidth the system is surprisingly robust. Reliable measurements of lifetimes down to the subns level can be performed at subsecond image acquisition speeds. The system is capable of discriminating between image features differing in lifetime by less than 100 ps.

The phase and modulation lifetime measurements agree well with one another, although for the latter precisions are significantly degraded at the shortest lifetimes.

Acknowledgements

The authors wish to thank Prof Paul French and Dr Daniel Elson (Blackett Laboratory, Imperial College, London, U.K.) for help with the TCSPC measurements and provision of equipment. J. Swartling acknowledges support by the Swedish Research Council.

Clemens Kaminski gratefully acknowledges personal support from the Leverhulme Trust, U.K.

Jonathan Frank and Clemens Kaminski acknowledge support for this work by EPSRC via a PLATFORM grant (GR/R98679/01). Jonathan Frank acknowledges support from the U.S.A. Department of Energy, Office of Basic Energy Sciences, Division of Chemical Sciences, Geosciences, and Biosciences.

This work was supported by grants received from the Royal Society, the EPSRC (Engineering and Physical Sciences Research Council, U.K.), and HEFCE (The Higher Education Funding Council for England, U.K.).

References

Ballew, R.M. & Demas, J.N. (1989) An Error Analysis of the Rapid Lifetime Determination. *Method. Anal. Chem*. **61**, 30–33.

Becker, W., Bergmann, A., Hink, M.A. *et al.* (2004) Fluorescence lifetime imaging by time-correlated single-photon counting. *Microsc. Res. Techn*, **63**, 58–66.

Becker, W., Hickl, H., Zander, C. *et al.* (1999) Time-resolved detection and identification of single analyte molecules in microcapillaries by time-correlated single-photon counting (TCSPC). *Rev. Sci. Instrum*. **70**, 1835–1841.

Benninger, R.K.P., Hofmann, O., McGinty, J., Requejo-Isidro, J., Munro, I., Neil, M.A.A., deMello, A.J. & French, P.M.W. (2005) Time-resolved fluorescence imaging of solvent interactions in microfluidic devices. *Optics Express*, **13**, 6275–6285.

Boddeke, F.R. (1998) Quantitative Fluorescence Microscopy. PhD Dissertation. Technische Universiteit Delft, The Netherlands).

Booth, M.J. & Wilson, T. (2004) Low-cost, frequency-domain, fluorescence lifetime confocal microscopy. *J. Microsc.-Oxf*. **214**, 36–42.

Calleja, V., Ameer-Beg, S.M. & Vojnovic, B. (2003) Monitoring conformational changes of proteins in cells by fluorescence lifetime imaging microscopy. *Biochem. J*. **372**, 33–40.

Clayton, A.H., Hanley, Q.S. & Arndt-Jovin, D.J. (2002) Dynamic fluorescence anisotropy imaging microscopy in the frequency domain (rFLIM). *Biophys. J*. **83**, 1631–1649.

Clegg, R.M., Jovin, T.M. & Gadella, T.W.J. (1994) Fluorescence lifetime imaging microscopy: Pixel-by-pixel analysis of phase-modulation data. *Bioimaging*, **2**, 139–159.

Dai, X., Eccleston, M.E., Yue, Z., Slater, N.K.H., & Kaminski, C.F. (2006) A Spectroscopic Study of the Self Association and Inter-Molecular Aggregation Behaviour of pH-Responsive poly (1-lysine iso-phthalamide). *Polymer*, **47**, 2689–2698.

Dasgupta, P.K., Eom, I.Y., Morris, K.J. *et al.* (2003) Light emitting diode-based detectors absorbance, fluorescence and spectroelectrochemical measurements in a planar flow-through cell. *Anal. Chim. Acta*, **500**, 337–364.

Denk, W., Strickler, J.H. & Webb, W.W. (1990) 2-Photon Laser Scanning Fluorescence Microscopy. *Science*, **248**, 73–76.

Dowling, K., Dayel, M.J., Hyde, S.C.W. *et al.* (1999) High resolution time-domain fluorescence lifetime imaging for biomedical applications. *J. Mod. Opt*. **46**, 199–209.

Dowling, K., Dayel, M.J., Lever, M.J., French, P.M.W., Hares, J.D. & Dymoke-Bradshaw, A.K.L. (1998) Fluorescence lifetime imaging with picosecond resolution for biomedical applications. *Optics Lett*. **23**, 810–812.

Dowling, K., Hyde, S.C.W., Dainty, J.C. *et al.* (1997) 2-D fluorescence lifetime imaging using a time-gated image intensifier. *Opt. Commun*. **135**, 27–31.

Dunsby, C., Lanigan, P.M.P., McGinty, J. *et al.* (2004) An electronically tunable ultrafast laser source applied to fluorescence imaging and fluorescence lifetime imaging microscopy. *J. Phys. D: Appl. Phys*. **37**, 3296–3303.

Eccleston, M.E., Kaminski, C.F., Slater, N.K.H. *et al.* (2004) Optical characteristics of responsive biopolymers; co-polycondensation of tri-functional amino acids and Cy-3 bis-amine with diacylchlorides. *Polymer*, **45** (1), 25–32.

Eccleston, M.E., Kuiper, M., Gilchrist, F.M. *et al.* (2000) pH-responsive pseudo-peptides for cell membrane disruption. *J. Controlled Release*, **69**, 297–307.

Elder, A.D., Swartling, J., Matthews, S.M. *et al.* (2006) Application of frequency-domain Fluorescence Lifetime Imaging Microscopy as a quantitative analytical tool for microfluidic devices. *Opt. Express*, **14**, 5456–5467.

French, T., Berland, W.M., Yu, K.M., Dong, C.Y., Gratton, E. & So, P.T.C. (1995) Time-resolved fluorescence microscopy using two-photon excitation. *Bioimaging*, **3**, 49–63.

Gadella, T.W.J., Jovin, T.M. & Clegg, R.M. (1993) Fluorescence Lifetime Imaging Microscopy (Flim) – Spatial- Resolution of Microstructures On The Nanosecond Time-Scale. *Biophys. Chem*. **48**, 221–239.

van Geest, L.K. & Stoop, K.W.J. (2003) FLIM on a wide field fluorescence microscope. *Lett. Peptide Sci*. **10**, 501–510.

Hanley, Q.S. & Clayton, A.H.A. (2005) A–B plot assisted determination of fluorophore mixtures in a fluorescence lifetime microscope using spectra or quenchers. *J. Microscopy*, **218**, 62–67.

Hanley, Q.S., Subramaniam, V., Arndt-Jovin, D.J. *et al.* (2001) Fluorescence lifetime imaging: multi-point calibration, minimum resolvable differences, and artifact suppression. *Cytometry*, **43**, 248–260.

Harris, J.M. & Lytle, F.E. (1977) Measurement of subnanosecond fluorescence decays by sampled single-photon detection. *Rev. Sci. Instrum*, **48**, 1470–1476.

Herman, P., Maliwal, B.P., Lin, H.J. *et al.* (2001) Frequency-domain fluorescence microscopy with the LED as a light source. *J. Microsc.-Oxf*. **203**, 176–181.

Kiyomiya, K., Matsuo, S. & Kurebe, M. (1999) Proteasome is a carrier to translocate doxorubicin from cytoplasm into nucleus. *Life Sci*. **62**, 1853–1860.

Köllner, M. & Wolfrum, J. (1992) How Many Photons Are Necessary For Fluorescence-Lifetime Measurements. *Chem. Phys. Lett*. **200**, 199–204.

Kress, M., Meier, T., El-Tayeb, T.A.A. *et al.* (2001) *Photon Migration, Opical Coherence Tomography, and Microscopy*, Vol. 2, pp. 108–113. Spie-Int. Society Optical Engineering, Bellingham.

Lakowicz, J.R. (1999) *Principles of Fluorescence Spectroscopy*, 2nd edn. Kluwer Academic/Plenum Publishers, New York.

Lakowicz, J.R. & Berndt, K.W. (1991) Lifetime-Selective Fluorescence Imaging Using An Rf Phase-Sensitive Camera. *Rev. Sci. Instrum.* **62**, 1727–1734.

Lakowicz, J.R., Szmacinski, H., Nowaczyk, K. *et al.* (1992) Fluorescence lifetime imaging. *Anal Biochem.* **202**, 316–330.

Lin, H.J., Herman, P. & Lakowicz, J.R. (2003) Fluorescence lifetime-resolved pH imaging of living cells. *Cytom. Part A*, **52A**, 77–89.

McGuinness, C.D., Sagoo, K., McLoskey, D. *et al.* (2004) A new sub-nanosecond LED at 280 nm: application to protein fluorescence. *Meas. Sci. Technol.* **15**, L19–L22.

Mitchell, A.C., Wall, J.E., Murray, J.G. *et al.* (2002) Direct modulation of the effective sensitivity of a CCD detector: a new approach to time-resolved fluorescence imaging. *J. Microsc.-Oxf.* **206**, 225–232.

van Munster, E.B., Gadella, T.W. Jr. (2004) Suppression of photobleaching-induced artifacts in frequency-domain FLIM by permutation of the recording order. *Cytometry A*, **58**, 185–194.

Mynbaev, D.K. & Scheiner, L.L. (2000) Fiber-optic communications technology. Prentice Hall, NJ.

van der Oord, C.J.R., Stoop, K.W.J. & van Geest, L.K. (2001) Chapter title. *Advances in Fluorescence Sensing Technology V*, Vol. 2, pp. 115–118. Spie-Int. Society Optical Engineering, Bellingham.

Periasamy, A., Wodnicki, P., Wang, X.F. *et al.* (1996) Time-resolved fluorescence lifetime imaging microscopy using a picosecond pulsed tunable dye laser system. *Rev. Sci. Instrum.* **67**, 3722–3731.

Philip, J. & Carlsson, K. (2003) Theoretical investigation of the signal-to-noise ratio in fluorescence lifetime imaging. *JOSA A*, **20**, 368–379.

Settersten, T.B., Dreizler, A. & Farrow, R.L. (2002) Temperature- and species-dependent quenching of CO *B* probed by two-photon laser-induced fluorescence using a picosecond laser. *J. Chem. Phys.* **117**, 3173–3179.

So, P.T.C., Dong, C.Y., Berland, K. *et al.* (1994) A 2-Photon Confocal Lifetime Microscope. *Biophys. J*, **66**, A276.

Squire, A., Verveer, P.J., Bastiaens, P.I. *et al.*(2000) Multiple frequency fluorescence lifetime imaging microscopy. *J. Microsc*, **197**, 136–149.

Suhling, K. (2006) Fluorescence Lifetime Imgaging. *Methods Express, Cell Imaging* (ed. D. Stephens), pp. 219–245. Scion publishing, Bloxham, U.K.

Szmacinski, H. & Lakowicz, J.R. (1995) Fluorescence lifetime-based sensing and imaging. *Sens. Actuator B-Chem.* **29**, 16–24.

vandeVen, M., Ameloot, M., Valeur, B. & Boens, N. (2005) Pitfalls and their remedies in time-resolved fluorescence spectroscpoy and microscopy. *J. Fluorescence*, **15**, 377–413.

Vermeer, J.E.M., Van Munster, E.B. & Vischer, N.O. (2004) Probing plasma membrane microdomains in cowpea protoplasts using lipidated GFP-fusion proteins and multimode FRET microscopy. *J. Microsc.-Oxf.* **214**, 190–200.

Volkmer, A., Subramaniam, V., Birch, D.J.S. *et al.* (2000) One- and two-photon excited fluorescence lifetimes and anisotropy decays of Green Fluorescent Proteins. *Biophys. J.* **78**, 1589–1598.